Research paper

Pattern Measurement of Large Antenna by Sequential Sampling Method in Cylindrical Near-Field Test

M. Karimipour*

Department of Electrical Engineering, Arak University of Technology, Arak, Iran.

Article Info	Abstract
    *Corresponding Author's Email Address: m.karimipour@arakut.ac.ir	**Background and Objectives:** Cylindrical scanning technique is a well-established indirect measurement method to characterize a wide range of antenna patterns such as fan-beam antennas and phased array antennas with versatile radiation patterns. **Methods:** Cylindrical scanning technique which is based on the nearfield-to-far-field transformation based on cylindrical mode coefficients (CMCs), cannot predict the antenna radiation pattern with a very narrow beamwidth in the azimuth plane accurately, because a remarkable error occurs during the calculation of the derivative of high-order Hankel functions in the CMCs extraction. We aim to address this issue and introduce a simple yet rigorous technique namely the sequential sampling method (SSM) in conjunction with the two-dimensional Fast Fourier Transform (2D-FFT) to efficiently calculate the far-field radiation pattern of a super-directive antenna with a very narrow beamwidth in the azimuth plane. Briefly, the SSM offers several sequences of progressive azimuth angles and the corresponding order of Hankel functions in such a way that CMCs fully span 360 degrees of azimuth angles (φ) in the cylindrical coordinate system in each sequence. Afterward, by putting the far-field obtained by these sequences together, the final radiation pattern will have a high angular resolution. This technique can also be applied to determine the necessary criteria in the data acquisition step which should be satisfied to precisely measure the radiation pattern of super-directive antennas. These criteria are the maximum acceptable sampling resolution and the minimum value of the required azimuth angle (φ) in the data acquisition step if the far-field pattern is merely desired on the front side of the antenna. **Results:** For verifications, the far-field radiation pattern of an electrically large slot array antenna including 81×15 slots is calculated at 8.75 GHz by the proposed technique and the results are compared with the array theory. The results show that the azimuth pattern can accurately be measured as small as 0.1° resolution by the SSM. **Conclusion:** By comparing the results obtained by the proposed method and the traditional cylindrical scanning method, it can be inferred that the far-field pattern of an antenna with narrow beamwidth in the azimuth plane can easily be characterized by a cylindrical scanning system without any huge computational burden.

Introduction

Nowadays, there are several methods to measure antenna radiation patterns [1]. These methods are divided into two categories, namely direct and indirect. In the direct method, the far-field pattern is measured without any intermediate step. Depending on the

electrical size of antenna, the measurement can be performed either in an indoor anechoic chamber or in free space. For a wide range of antennas, it is not possible to measure the far-field radiation pattern directly. The main reason is the large electrical size of these antennas and the corresponding far zone region. For example, the size of antennas in phased array radars is approximately several wavelengths.

Therefore, the far-field region of these radiators will be more than several hundred meters. In this condition, setting up the far-field measurement system is a very complex and costly process. Therefore, measured results may not be valid due to several inevitable errors that may occur during the data acquisition. To overcome this drawback, indirect measurement methods have been introduced. In the indirect methods, some post-processing algorithms must be performed to determine the electromagnetic radiation pattern with high accuracy [2]. These post-processing algorithms are configured based on the kind of data acquisition. According to the geometric shape where the data are acquired, three well-established techniques, including planar, cylindrical, and spherical near-field measurements are introduced. Although, several other techniques such as data sampling over arbitrary geometries or curvatures are also reported in the literature [3]. These techniques are applied for special purposes.

Each of the aforementioned near-field methods is useful for testing a particular antenna. For example, the planar near-field method is useful for testing high directive antennas with a nontrivial front-to-back ratio of the pattern. When it is necessary to evaluate the radiation behavior of the antenna on the backside, the cylindrical near-field (CNF) system is a very useful solution. In most cases, the radiation pattern of array antennas with large size in the elevation plane and medium size in the azimuth plane can easily be measured by cylindrical scanning systems [2]. Conversely, the spherical near-field systems are useful to characterize medium and low-gain antennas with omnidirectional and isotropic-like patterns.

In the cylindrical scanning system, which is the case in this paper, the near-field data of the antenna under test (AUT), including amplitude and phase of electric fields, are acquired over a right circular cylinder or a cone-shape area via a simple probe. In practice, the acquisition process is performed by employing some measurement equipment and optical instruments (such as a laser tracker [1]) if high accuracy is needed. In the computational step as a post-processing task, the near-field to far-field transformation is performed to characterize the antenna pattern [4]-[8]. There are two main techniques including 2D-FFT and the matrix method to describe the far-field pattern from near-field information. The first one is fast, very efficient, and almost accurate [7], however, the near-field data should be acquired in a uniform grid. Meanwhile, the latter can be implemented for nonuniform sampling, and therefore it is a very suitable solution for considering probe position error during the data acquisition [8], [9]. The main disadvantage of the matrix method is the high computational cost of post-processing, which is unsuitable for pattern measurement of electrically large size antennas. Both techniques benefit from the description of electromagnetic fields outside the antenna by orthogonal basis functions namely cylindrical waves. If the sampling grid is regular, 2D-FFT can be efficiently applied to calculate the unknown coefficients of basis functions or CMCs. Afterward, the far-field pattern can easily be described by the 1D-FFT routine. Meanwhile, if the sampling grid is nonuniform, the derivation of the far-field pattern can be performed using the matrix operations [9] or interpolating the irregular NF data into regular [10], [11]. As pioneers in the field, AMETEK NSI-MI is the world leader in near-field measurements and produce a full range of standard and customized measurement system for certain applications [12]. NSI-MI says that the cylindrical near-field measurement system is useful to measure broad beams in the azimuth plane such as fan beams. In other words, the beamwidth of the azimuth pattern is a restricted factor for using the CNF system.

The basic theory behind the CNF systems expresses that the process of the far-field reconstruction pattern with an angular resolution of less than 0.5° in the azimuth plane involves describing near-field data with very high-order cylindrical basis functions [1]. In this fashion, the calculation of high-order CMCs corresponding to orthogonal basis functions may be associated with some errors. For example, the authors in [13] used a nearly huge grid including 512 samples on the φ-axis and 156 samples on the z-axis to accurately measure the far-field pattern of a very large L-band radar antenna. In this measurement, the maximum cylindrical mode function is in order of 256 which leads to the azimuth angular resolution of 0.7°. If the smaller resolution in the azimuth plane is necessary, the higher order of CMCs and Hankel function is required.

In this paper, a simple yet rigorous approach based on the SSM in conjunction with 2D-FFT is introduced to efficiently calculate the far-field radiation pattern with a very narrow beamwidth in the azimuth plane. The SSM offers several sequences of progressive azimuth angles along with the corresponding order of Hankel functions so that CMCs fully span 360 degrees for azimuth angles (φ) in each sequence. Afterward, by putting the far-field patterns obtained by these sequences together, the final radiation pattern will have a high angular resolution. We show that if these sampled sequences are arranged

together, the final resolution of the measured pattern in the azimuth plane would be as small as 0.1°. As an advantage of the proposed method, the monopulse antenna with a difference beam pattern in the azimuth plane can be rigorously measured with the accuracy of null position detection smaller than 0.1°.

To verify the concept, a 25×81 slot array antenna is considered as the AUT and the near-field data over a conceptual cylinder around the antenna is calculated via an ideal isotropic probe. The AUT is considered in the YZ plane such that the 81 elements are aligned on the y-axis. By modeling the radiation behavior of each slot by a finite-length magnetic dipole, a comprehensive mathematical framework is implemented to determine the radiation behavior of the entire slots in the array environment with every excitation distribution for slots provided that negligible mutual coupling exists between the slots. The proposed model enables the calculation of electromagnetic waves in both near-field and far-field regions. Therefore, the obtained results by the proposed model can also be employed to evaluate the near-field to far-field transformation algorithm developed by the SSM.

Analytical Model for Data Acquisition

The proposed model makes it possible to describe the radiated field of any slot or microstrip array in an arbitrary geometrical arrangement, flat or conformal, provided that the radiative behavior of the co-polarization (Co-Pol) and cross-polarization (Cross-Pol) components of the antenna can be modeled analytically. In addition, the model will be able to evaluate the radiated field in any desired area such as flat plane, cylinder, spherical, or even other conformal geometries such as cone. Therefore, one can employ it to verify the spherical scanning system as well. Note that this analytical method neglects the mutual coupling between the radiating elements in the array environment, hence, the model is valid while the coupling among the elements is negligible [14]. It is worth noting that the CADFEKO 2021 software is also able to calculate near-field waves around the antenna on a flat, cylindrical, spherical, and even cone areas. Therefore, it can be employed for data acquisition as well.

A. Theoretical Formulation

The radiation behavior of a single slot and microstrip patch can roughly be modeled by a magnetic and electric dipole, respectively. This model is also valid when these elements are arranged in an array configuration provided that the mutual coupling between elements is negligible. Therefore, the calculation process of electric and magnetic fields surrounding the dipole array with any arrangement leads to establishing a comprehensive analytical model for evaluating the radiation pattern of slot and microstrip array antennas. First, the mathematical formulation is introduced for the model,

afterward, the model is verified by a case study simulated in the CST software.

According to the array theory, the electric field at any observation point in the free space can be described as the superposition of electric fields radiated from all elements. It is well-known that the electric field radiated by an electric and magnetic dipole which are aligned in the z-direction are as follows [15]:

$$Electric\ Dipole: E_\theta = G_\theta . I \qquad (1)$$

$$Magnetic\ Dipole: E_\varphi = G_\varphi . I \qquad (2)$$

where, G_θ is simply defined as below.

$$G_\theta = -j\eta \frac{e^{-jk_0 r_f}}{2\pi r_f} \left[\frac{cos\left(\frac{k_0 d_f}{2}cos\theta_f\right) - cos\left(\frac{k_0 d_f}{2}\right)}{sin\theta_f} \right] \qquad (3)$$

Similarly, $G_\varphi = -G_\theta/\eta$. In (3), k_0 is the free space wavenumber, d_f is the dipole length which is greater than $\lambda/10$, (λ is the wavelength). The parameter η is the characteristic impedance in the free space and finally θ_f is the angular parameter defined in the spherical local coordinate system.

Equations (1) up to (3) are defined at the local coordinate system associated with each dipole element, i.e., (x_f, y_f, z_f) (See Fig. 1). To express the radiated field of the element in the global coordinate system, i.e., (x_g, y_g, z_g), one can employ the coordinate transformation technique presented in [16], and decompose the excitation current component of each dipole element into three components, I_x, I_y, I_z. Finally, regarding dipole directions, the electric field associated with each element is determined in every observation point in the global rectangular coordinate system. This scenario can be applied to every radiating element (including magnetic and electric dipole elements).
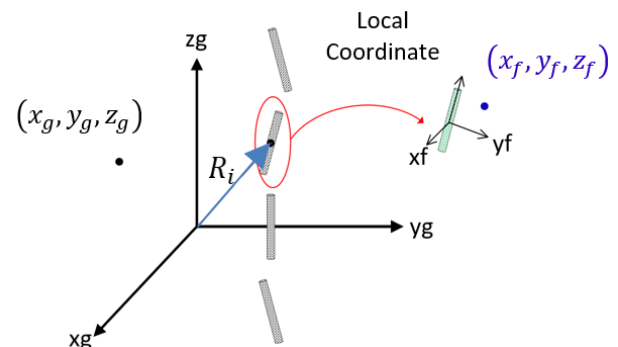
Fig. 1: General dipole array configuration along with the local and global coordinate system.

Using the superposition principle, the electric field radiated by all elements can be obtained at any arbitrary observation point.

Therefore, the general form of (1) can be represented in the matrix form as follows:

$$\begin{bmatrix} [E_x]_{N_s \times 1} \\ [E_y]_{N_s \times 1} \\ [E_z]_{N_s \times 1} \end{bmatrix} =$$

$$\begin{bmatrix} [G_{xx}]_{N_s \times N_d} & [G_{xy}]_{N_s \times N_d} & [G_{xz}]_{N_s \times N_d} \\ [G_{yx}]_{N_s \times N_d} & [G_{yy}]_{N_s \times N_d} & [G_{yz}]_{N_s \times N_d} \\ [G_{zx}]_{N_s \times N_d} & [G_{zy}]_{N_s \times N_d} & [G_{zz}]_{N_s \times N_d} \end{bmatrix} \begin{bmatrix} [I_x]_{N_d \times 1} \\ [I_y]_{N_d \times 1} \\ [I_z]_{N_d \times 1} \end{bmatrix} \quad (4)$$

The conversion blocks, $[G_{ij}]_{N_s \times N_d}$, in (4) are defined to convert the dipole current in the 'j' direction to the electric field component along the 'i' direction. For example, if a specific dipole is aligned to the x-direction, all entries of conversion blocks, $[G_{ij}]_{N_s \times N_d}$, associated with that element are zero except the ones with $[G_{ix}]_{N_s \times N_d}$ indices. The parameters N_d and N_s are the number of dipoles and observation points, respectively. The derivation scenario of [G] blocks is summarized as follows:

- Determine $x_{g,NF}$, $y_{g,NF}$ and $z_{g,NF}$ according to the near-field sampling area. (For example, cylinder in this case)
- Determine r_g, θ_g and ϕ_g in the spherical coordinate system as follows:

$$(\theta_g, \phi_g) = \left(tan^{-1}\left(\frac{\sqrt{x_g^2 + y_g^2}}{z_g} \right), tan^{-1}\left(\frac{y_g}{x_g} \right) \right)$$

$$r_g = \sqrt{x_g^2 + y_g^2 + y_g^2}$$

- Decompose each dipole to three dipoles along the x, y, and z-directions.
- Following [16] and determining the type of transfer matrix, namely $\Re$, for these three decomposed components which are defined for each dipole. For example: $\Re_{XZX}, \Re_{ZXZ}, \Re_{ZYZ}$ or $\Re_{XYZ}$, where the $[\Re_{ijk}]$ denotes the rotation matrix around k, j, and i axes, respectively. This process should be done element by element in the array. It is worth noting that the dipole direction is the only determinative factor to use what form of $[\Re_{ijk}]$ needs to describe the electromagnetic behavior of dipole. The matrix, $[\Re_{ijk}]$, can be determined by multiplying three rotation matrices which are constructed from three decomposed components of the excitation current vector along the x-, y-, and z-directions. These three rotation matrices are defined based on the Euler angles α, β, γ. In the following, two forms of $[\Re_{ijk}]$ are described based on the Euler angles [16]:

$$\Re = \Re_{XZX}(\alpha, \beta, \gamma)$$
$$= \begin{bmatrix} \cos\gamma & \sin\gamma & 0 \\ -\sin\gamma & \cos\gamma & 0 \\ 0 & 0 & 1 \end{bmatrix} \begin{bmatrix} 1 & 0 & 0 \\ 0 & \cos\beta & \sin\beta \\ 0 & -\sin\beta & \cos\beta \end{bmatrix}$$
$$\begin{bmatrix} \cos\alpha & \sin\alpha & 0 \\ -\sin\alpha & \cos\alpha & 0 \\ 0 & 0 & 1 \end{bmatrix}$$

$$\Re = \Re_{ZYZ}(\alpha, \beta, \gamma)$$
$$= \begin{bmatrix} \cos\gamma & \sin\gamma & 0 \\ -\sin\gamma & \cos\gamma & 0 \\ 0 & 0 & 1 \end{bmatrix} \begin{bmatrix} \cos\beta & 0 & \sin\beta \\ 0 & 1 & 0 \\ -\sin\beta & 0 & \cos\beta \end{bmatrix}$$
$$\begin{bmatrix} \cos\alpha & \sin\alpha & 0 \\ -\sin\alpha & \cos\alpha & 0 \\ 0 & 0 & 1 \end{bmatrix}$$

Accordingly, as shown in (4), three components of G are required to fully characterize the electromagnetic behavior of the dipole aligned in an arbitrary direction.

- Transfer the near-field points in the global coordinate system ($x_{g,p}$, $y_{g,p}$ and $z_{g,p}$) to the local coordinate system associated with the mn^{th} element as follows:

$$x_{f,p} = \Re_{11}(x_{g,p} - x_{e,m}) + \Re_{12}(y_{g,p} - y_{e,m}) + \Re_{13}(z_{g,p} - z_{e,m})$$
$$y_{f,p} = \Re_{21}(x_{g,p} - x_{e,m}) + \Re_{22}(y_{g,p} - y_{e,m}) + \Re_{23}(z_{g,p} - z_{e,m})$$
$$z_{f,p} = \Re_{31}(x_{g,p} - x_{e,m}) + \Re_{32}(y_{g,p} - y_{e,m}) + \Re_{33}(z_{g,p} - z_{e,m})$$

where p denotes the number of observation points in the near-field region and m is the element numbers in the array environment. In addition, the subscript g and f denote the local and global coordinate systems, respectively.

- Determine $r_{f,p}, \theta_{f,p}$ and $\phi_{f,p}$ in the spherical coordinate system from $x_{f,p}$, $y_{f,p}$ and $z_{f,p}$.
- Calculate $G_{f,\theta}$ and $G_{f,p}^{\phi}$ for magnetic dipole are as follows [15]:

$$G_{f,p}^{\theta} = -j\eta \frac{e^{-jk_0 r_{f,p}}}{2\pi r_{f,p}} \left[\frac{\cos\left(\frac{k_0 d_{f,p}}{2}\cos\theta_{f,p}\right) - \cos\left(\frac{k_0 d_{f,p}}{2}\right)}{\sin\theta_{f,p}} \right],$$
$$G_{f,p}^{\phi} = 0$$

- Calculate $G_{f,p}^x$, $G_{f,p}^y$ and $G_{f,p}^z$ from $G_{f,p}^\theta$ and $G_{f,p}^\phi$ components determined in the previous step.
- Transform $G_{f,p}^x, G_{f,p}^y$ and $G_{f,p}^z$ to the global coordinate system $G_{g,p}^x$, $G_{g,p}^y$ and $G_{g,p}^z$, as follows:

$$G_{g,p}^x = \mathbb{Q}_{11}G_{f,p}^x + \mathbb{Q}_{12}G_{f,p}^y + \mathbb{Q}_{13}G_{f,p}^z$$
$$G_{g,p}^y = \mathbb{Q}_{21}G_{f,p}^x + \mathbb{Q}_{22}G_{f,p}^y + \mathbb{Q}_{23}G_{f,p}^z$$
$$G_{g,p}^z = \mathbb{Q}_{31}G_{f,p}^x + \mathbb{Q}_{32}G_{f,p}^y + \mathbb{Q}_{33}G_{f,p}^z$$

where $[\mathbb{Q}] = [\Re]^{-1}$.

Following the above guideline, all entries of coefficient matrix ($[G]$) represented in (4) are determined whose dimension is $3N_s \times 3N_d$. The factor 3 observed in the matrix dimension returns to the three decomposed components of each dipole in the array antenna.

B. Verification of the Analytical Model for Data Acquisition

As an example, the radiation behavior of the array shown in Fig. 2(a) is characterized by the proposed model. 50 elements of magnetic dipoles are placed together in the YZ plane with θ angles shown in Fig. 2(b) The θ angles are defined relative to the z-axis. The working frequency and dipole spacing are considered to be 8.75GHz and

24mm, respectively. The current magnitudes of the dipoles are set in the form of Taylor distribution with a side-lode level (SLL) of -40dB and $\bar{n} = 4$ [15]. The progressive phases of the dipoles are set to zero, hence, the main beam of the pattern is aligned at $\theta = 90°$. Fig. 3 shows the [G] tensor defined in (4) as well as the far-field co-pol and cross-pol of the pattern at $\theta = 90°$. It is worth noting that an interesting application of this analytical model is to solve the inverse problem and extract the dipole currents from known E-field distribution around the array (which can be obtained by planar near-field measurement). As such, the *array calibration* can also be performed by this method. That is, by sampling the near-field around the antenna and finding the amplitude and phase of excitation current of the elements, it is possible to compare the real state of every element in the array configuration with their ideal states, and then, appropriate modifications can be adopted for faulty elements.

Position of Magnetic Dipoles (Element Numbers=50)

(a)

(b)
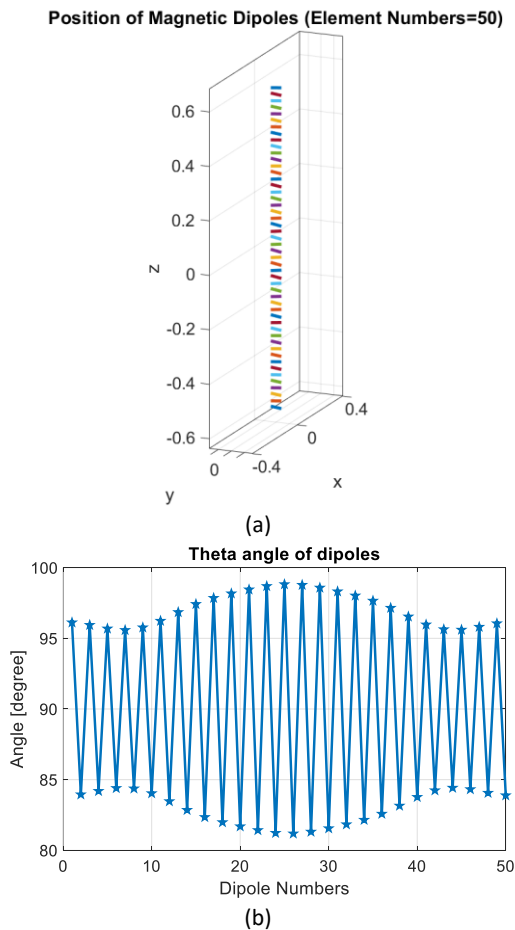
Fig. 2: (a) Dipole array configuration. (b) The values of θ angles relative to the z-axis for determining the element directions.

To further verify the proposed method, a 50-element slot array antenna with slot angles defined in Fig. 2(b) is simulated by the time-domain solver in the CST software, and the electric field data is extracted on a line at x=10 cm. In addition, the far-field pattern of the antenna is

simulated and recorded in $\varphi = 0°$ plane for comparison with the results obtained by the theoretical model. The theoretical model is established by arranging 50 elements of magnetic dipoles together in such a way that the dipole directions are exactly aligned to the slot directions and dipole center positions coincide with slot centers. Dipole currents can be obtained by solving the inverse problem, $\bar{I} = \bar{\bar{G}}^{-1}\bar{E}_{NF}$, where $\bar{E}_{NF}$ is the near-field data extracted from the CST software. In the next step, the far-field pattern of the antenna is calculated by the theoretical model. This is simply accomplished by considering the observation points (r_g, θ_g and ϕ_g) in the far zone on the $\varphi = 0°$ plane.

(a)

(b)

(c)
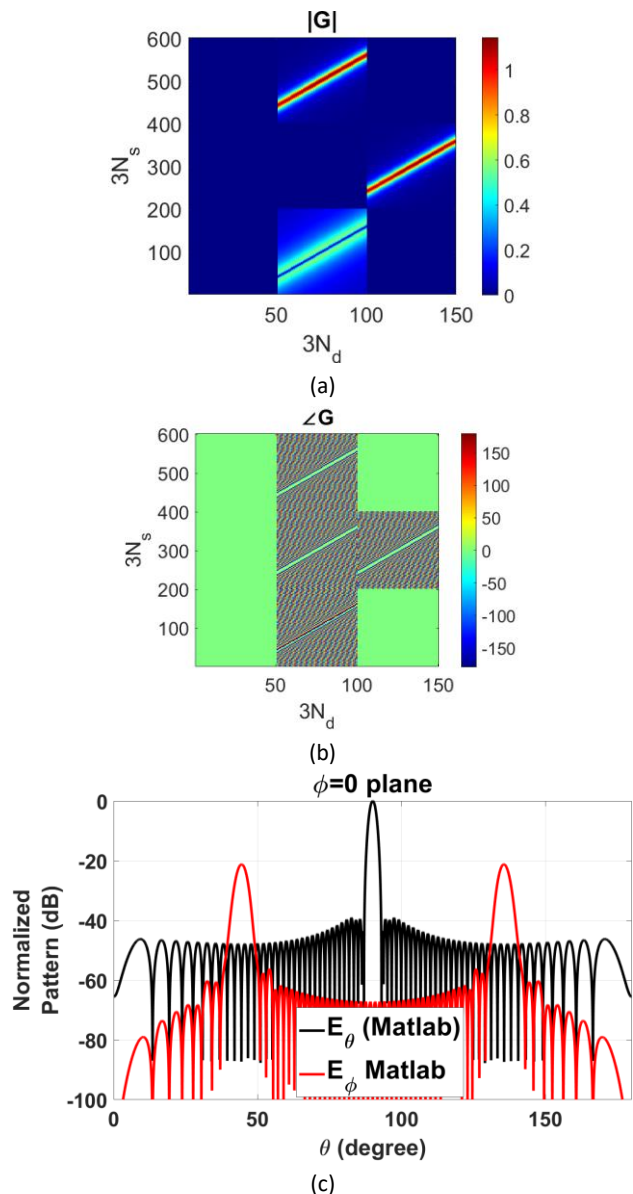
Fig. 3: (a) Amplitude and (b) phase of [G] tensor for antenna configuration shown in Fig. 2. (c) Calculated far-field radiation pattern on the $\phi = 0°$ plane.

Fig. 4 shows the simulation setup in the CST software to extract $\bar{E}_{NF}$ and the far-field pattern. The comparison

of the far-field pattern obtained by the CST software and the theoretical model is presented in Fig. 5. The results show that the proposed model enables to fully characterize the slot array antenna pattern. Therefore, the analytical model for data acquisition is prepared to extract the near-field data on a cylinder, which is a crucial step for setting up a CNF system.

Fundamentals of CNF Measurement Technique

The electromagnetic waves around an arbitrary antenna can be described by a set of CMCs as follows [1]:
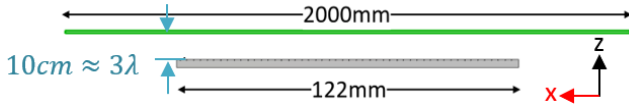
Fig. 4: Characterization of slot array radiation pattern by sampling nearfield data over the line at x=10 cm.
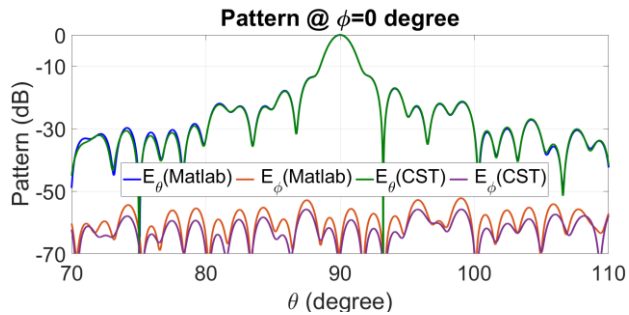
Fig. 5: The comparison between the far-field pattern of the slot array extracted from the theoretical model and the full-wave simulation.

$$E_z^{NF}(\varphi, z) =$$
$$\sum_{n=-M}^{M} \int_{-\infty}^{+\infty} b_n(k_z) \frac{k_\rho^2}{k_0} H_n^{(2)}(k_\rho a) e^{jn\varphi} e^{-jk_z z} \, dk_z \quad (5)$$

$$E_\varphi^{NF}(\varphi, z) = \sum_{n=-M}^{M} \int_{-\infty}^{+\infty} \left\{ b_n(k_z) \frac{nk_z}{ak_0} H_n^{(2)}(k_\rho a) - \right.$$
$$\left. a_n(k_z) \frac{\partial H_n^{(2)}(k_\rho r)}{\partial r} \Big|_{r=a} \right\} e^{jn\varphi} e^{-jk_z z} \, dk_z \quad (6)$$

In (5) and (6), n is the mode index and M is the maximum number of modes that should be defined based on the accuracy of the calculations in the φ direction. The parameter a is the scanner cylinder radius. According to [1], $M = k_0 r_t + M_0$ where r_t is the minimum radius of a conceptual cylinder encompassed the AUT and M_0 is chosen larger than 10 corresponding to the required accuracy. For example, the pattern measurement of a large antenna with small beamwidth in the φ direction, requires a large number of CMCs for the far-field calculations.

As stated in [1], since the maximum separation among the sampling data in the φ direction is forced by $\Delta\varphi \leq \frac{\pi}{M}$, we do not have freedom for choosing number of modes and data sampling steps in the φ direction, simultaneously. Therefore, to measure the patterns with narrow beamwidth in the azimuth plane, first, it should be

selected the desired φ steps and, then determined the maximum mode number. The radial wavenumber, k_ρ, in (5) and (6) is equal to $\sqrt{k_0^2 - k_z^2}$, where $k_z = -\frac{\pi}{\Delta z_{scan}} + \frac{2m\pi}{n_{k_z} \Delta z_{scan}}$ and $m = [0, n_{k_z} - 1]$. The parameter n_{k_z} is the number of points in the spectral domain along the z-axis which is in the form of $2^q (q > 9)$. The coefficients $a_n(k_z)$ and $b_n(k_z)$ in (5) and(6) are CMCs which can easily be obtained by some mathematical manipulations [1]:

$$b_n(k_z) = \frac{k_0}{k_\rho^2 H_n^{(2)}(k_\rho a)} \mathcal{E}_v(n, k_z) \quad (7)$$

$$a_n(k_z) = \frac{1}{\frac{\partial H_n^{(2)}(k_\rho r)}{\partial r}\Big|_{r=a}} \left[b_n(k_z) \frac{nk_z}{ak_0} H_n^{(2)}(k_\rho a) - \right.$$
$$\left. \mathcal{E}_H(n, k_z) \right] \quad (8)$$

Equations (7) and (8) show that CMCs are obtained in matrix form, that is $[a_n]_{n_{k_z} \times n}$ and $[b_n]_{n_{k_z} \times n}$. The quantities, $\mathcal{E}_v(n, k_z)$, and $\mathcal{E}_H(n, k_z)$ are the spectral components of the tangential near-field data on the sampling cylinder as follows [1]:

$$\mathcal{E}_{v|H}(n, k_z) =$$
$$\frac{1}{4\pi^2} \int_{-\infty}^{+\infty} \int_{-\infty}^{+\infty} E_{z|\varphi}^{NF}(\varphi, z) \, e^{-jn\varphi} e^{jk_z z} d\varphi dk_z =$$
$$\frac{1}{4\pi^2} fftshift \left(FFT2 \left(E_{z|\varphi}^{NF}(\varphi, z), n_{k_z}, n \right) \right) \quad (9)$$

Finally, the far-field components of electric fields can be described based on CMSs as follows [1]:

$$E_\theta^{FF}(\theta, \varphi) =$$
$$-2jk_0 \sin\theta \frac{e^{-jk_0 R}}{R} \sum_{n=-N}^{N} j^n b_n(k_0 \cos\theta) e^{jn\varphi} =$$
$$-2jk_0 \sqrt{1 - \frac{k_z^2}{k_0^2}} \frac{e^{-jk_0 R}}{R} \mathbb{C}[fft(b_n(k_0 \cos\theta) e^{jn\varphi})] \quad (10a)$$

$$E_\varphi^{FF}(\theta, \varphi) =$$
$$-2jk_0 \sin\theta \frac{e^{-jk_0 R}}{R} \sum_{n=-N}^{N} j^n a_n(k_0 \cos\theta) e^{jn\varphi} =$$
$$-2jk_0 \sqrt{1 - \frac{k_z^2}{k_0^2}} \frac{e^{-jk_0 R}}{R} \mathbb{C}[fft(a_n(k_0 \cos\theta) e^{jn\varphi})] \quad (10b)$$

In the above equations, the operator FFT2 is the two-dimensional Fast Fourier transform which can be efficiently evaluated by MATLAB software with a computational burden of $N(logN)$. Similarly, the operator "$fftshift$" is employed to shift the zero-frequency component to the center of the spectrum in MATLAB.

The operator $\mathbb{C}$ in (10b) returns the Fourier transform of each row of a_n matrix. As can be seen in (9), and (10) both near-field data extraction and the far-field pattern reconstruction processes can be performed by the Fast Fourier technique, (the two-dimensional form for the near-field data extraction and the one-dimensional form for the far-field calculation).

Sequential Sampling Method

A. Basic Concept

During the computation of CMCs in the CNF system, it is necessary to keep in mind that the choice of the sampling steps along the φ direction or, equivalently, the choice of mode numbers should be done in such a way that the cylindrical basis functions span a full cycle of 360°, without any overlap or gap among the samples [1]. The discussion presented in the previous section shows that when the sampling process in the φ direction is done with very small steps, e.g., 0.1°, it means that the parameter n in (5) and (6) should be selected in the interval $[-1800, 1800]$. This guarantees a full span of 360° in the azimuth plane by the steps of 0.1°. In other words, the derivative of Hankel-function type two should be calculated for mode numbers up to 1800. Our investigations show that the MATLAB software can return the values of the derivative of Hankel-function type two by a maximum mode number of 500 with negligible error. This mode number corresponds to the sampling step of 0.36° in the φ direction. This bottleneck restricts the capability of the CNF system. That is why the CNF system is almost applied to measure specific antennas with relatively wide beamwidth in the φ direction. If needed, the interpolation technique is used in classical approaches to obtain better results in the φ direction [1], [17]-[19]. However, in most cases, the interpolation is unable to accurately predict the antenna pattern at some angles where sharp variations occur in the beam such as the null position in the monopulse patterns.

Closer examination of (5) up to (10) makes clear the fact that the far-field pattern obtained by the CNF measurement system in the φ direction is in discrete summation form of electric fields, that is, the measured far-field pattern is calculated at those points that are sampled in the φ direction. For example, if the near-field data are recorded in the φ direction by 0.2° steps, the final measured pattern has a resolution of 0.2°. This is in contrast to the measured pattern in the z-direction (or elevation plane). In fact, the accuracy of the pattern in the z-direction can be enhanced by simply padding the near-field data in the z-direction. (See (9)). According to this fact, the far-field pattern in the φ direction can be reconstructed by a repetitive routine in which the high-resolution pattern is constructed part by part. To do this, we offer the sequences of sampling points in the φ direction to obtain the fine resolution yet keep the accuracy of the computation (by limiting the mode numbers to 500 or smaller). To better explain the proposed method, let us assume that the required accuracy of the measured pattern in the φ direction is 0.1°. (b)

Fig. 6 depicts the proper sequences of the φ angles where the near-field to-far-field transformation should be performed for each sequence to obtain P_i. By putting the P_i patterns together, the resulted pattern has a fine resolution as desired (i.e., 0.1°). As can be seen in Fig. 6, the data acquisition process should be accomplished with the desired resolution to provide the required data for each sequence. In the next step, the number of sequences, N_{seq}, should be determined based on $\Delta\varphi_{seq}$. In this regard, it can be expressed the number of sequences as follows:

$$N_{seq} = \frac{\Delta\varphi_{seq}}{\Delta\varphi_{Data\ acquisition}} = \frac{0.5}{0.1} = 5 \qquad (11)$$

Acquisition data	0	0.1	0.2	0.3	0.4	0.5	....
	300	...	359.7	359.8	359.9		
M_Total	1800						

(a)

Sequence Number	Phi angles to calculate i^{th} pattern relating to the ith sequence						
Step 1	0	0.5	1	1.5	2	...	359.5
	Maximum Mode Number: $M_{seq1} = 360$						
	Calculated Far-field Patter= P_1						
Step 2	0.1	0.6	1.1	1.6	2.1	...	359.6
	Maximum Mode Number: $M_{seq2} = 360$						
	Calculated Far-field Patter= P_2						
Step 3	0.2	0.7	1.2	1.7	2.2	...	359.7
	Maximum Mode Number: $M_{seq3} = 360$						
	Calculated Far-field Patter= P_3						
Step 4	0.3	0.8	1.3	1.8	2.3	...	359.8
	Maximum Mode Number: $M_{seq4} = 360$						
	Calculated Far-field Patter= P_4						
Step 5	0.4	0.9	1.4	1.9	2.4	...	359.9
	Maximum Mode Number: $M_{seq5} = 360$						
	Calculated Far-field Patter= P_5						

(b)

Fig. 6: (a) The φ angle values needed for the data acquisition process by the SSM. (b) Proper φ angle sequences to limit the maximum mode numbers to 360 which leads to the calculation of P_i pattern with a high accuracy in MATLAB.

B. Verification of the SSM for Sum Pattern

To confirm the advantage of the SSM, a slot-array antenna including 25 rows and 81 columns is considered as the AUT (See Fig. 7). As shown in Fig. 7, the elements are located on the YZ plane. Since all 81 elements are in

the Y-axis direction, the antenna beamwidth in the azimuth plane will be narrow (about 1.4°), and hence, this is a good case to benchmark the SSM advantage. The working frequency is considered 8.75 GHz with the corresponding wavelength around 34 mm. The distance between each of the 81 elements in each row is 21.5mm. The width of each slot is equal to 2 mm. The separation among rows is 15 mm.

Therefore, the antenna dimension is 1.72 m × 0.36 m. The angle of slots with respect to the z-axis is determined by following the design method presented in [14]. Discussion about the slot array design method goes beyond the scope of the present paper.

Note that in a practical cylindrical scanner, the data acquisition process can be performed by rotating the AUT through a rotary positioner and moving a standard probe along the z-axis. The CNF configuration including the sampling points in the near-field region, where the tangential electric fields should be recorded, is shown in Fig. 7. The near-field components of the electric fields on the cylinder can be theoretically calculated by following the procedure outlined in the previous section. The radius of the scanning cylinder is considered to be 1.15m to avoid any physical contact between the antenna and probe during the data acquisition.

Fig. 8 shows the tangential electric field components of the slot array at 8.75 GHz which are depicted on the sampling cylinder. The height of the cylinder is considered as 2m to cover an acceptable angular range for the pattern in the elevation plane. As can be seen in Fig. 8, the peak values of the near-field components occur at the boresight direction, therefore, it is expected that the main beam of the far-field pattern is aligned in the boresight direction.
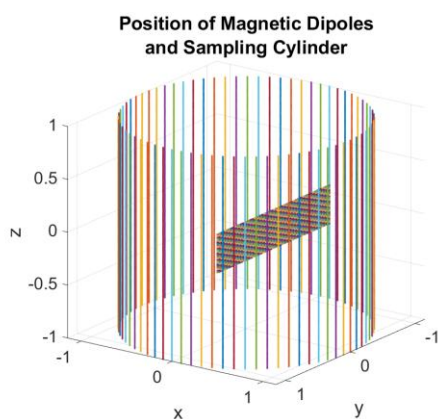
Fig. 7: Cylindrical sampling configuration developed in MATLAB.

According to the antenna dimensions, the maximum mode number is $M \approx 186$ assuming $M_0 = 10$, which leads to $\Delta\varphi < 0.96°$. Near-field-to-far-field transformation by the use of the sampling data with the step of $\Delta\varphi = 0.9°$ is accomplished in the azimuth plane.

The results are shown in Fig. 9a. It can be observed that the measured pattern cannot follow the overall behavior of the desired pattern, especially in sidelobe regions and so the results are not satisfactory. If $\Delta\varphi = 0.5°, 0.1°$ corresponding to $M = 360, 1800$, the measured patterns obtained by the CNF system are shown in Fig. 9(b) and Fig. 9(c), respectively.

The reduction of the sampling step should naturally increase the accuracy of antenna pattern measurement, but this has not happened. This problem is solved by properly using the SSM.
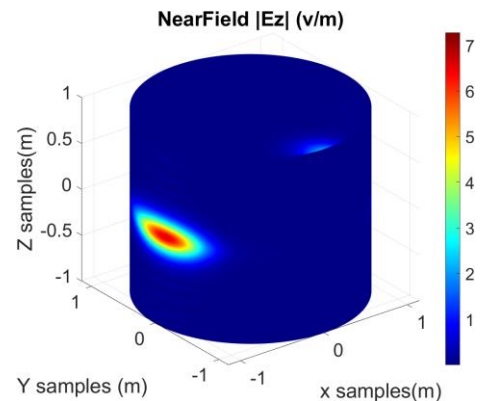
(a)
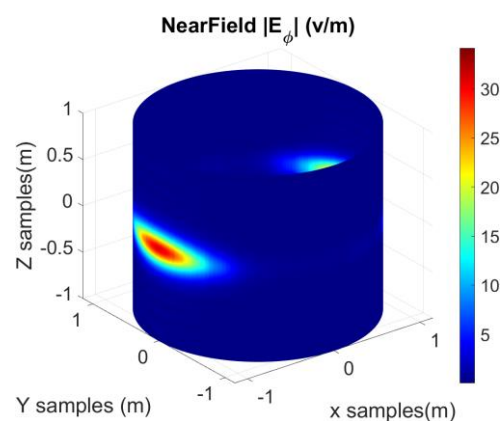
(b)

Fig. 8: Tangential electric field components of the slot array at 8.75 GHz. The sampling step in the φ and z directions are 0.1° and 1 mm, respectively. Note that the sampling step in the z-direction should satisfy the Nyquist theorem that is smaller than half of the wavelength.

The results obtained by employing the SSM are shown in Fig. 10 which confirm the usefulness of applying the SSM in the CNF measurement system. Note that the far-field patterns represented in Fig. 9 and Fig. 10 with the label 'array theory' are calculated by the same algorithm developed for near-field data acquisition. The difference is that (x_g, y_g, z_g) are defined in far-field region similar to that presented in Fig. 3.

(a)

(b)

(c)
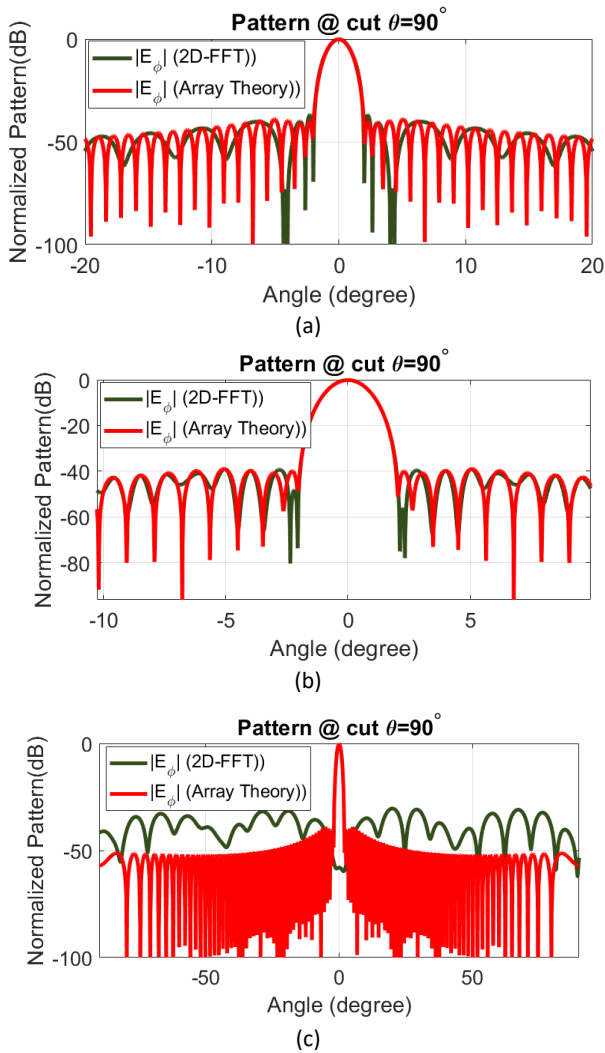
Fig. 9: The comparison between the far-field results obtained by the ideal array theory and the CNF system without using the SSM. The parameter $\Delta\varphi$ is considered as (a) 0.9° (b) 0.5° (c) 0.1°.

(a)

(b)

(c)

(d)

(e)
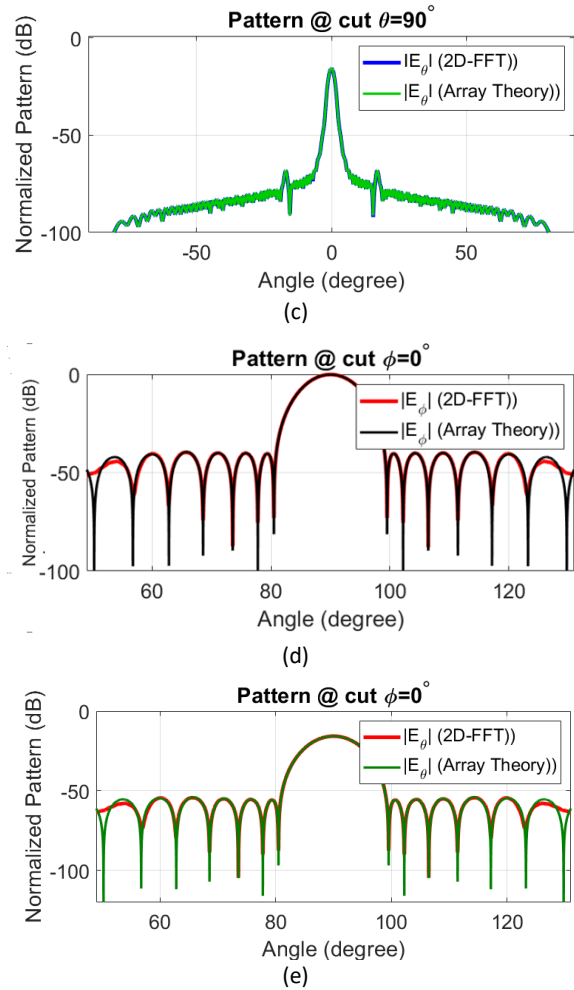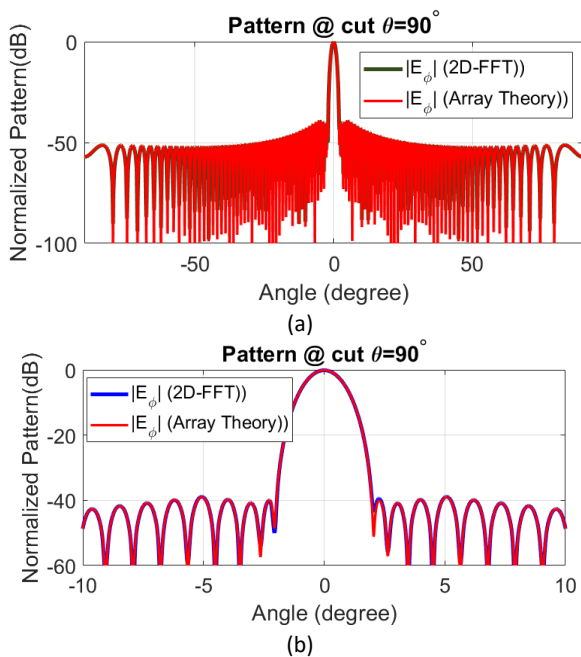
Fig. 10: The comparison between the far-field results obtained by the ideal array theory and the CNF system by using the SSM. $\Delta\varphi_{Data\ acquisition} = 0.1°$, $\Delta\varphi_{seq} = 0.5$, and $N_{seq} = 5$. (a) $|E_\varphi|$ at $\theta = 90°$. (b) closer view of $|E_\varphi|$ at $\theta = 90°$. (c) $|E_\theta|$ at $\theta = 90°$ (d) $|E_\varphi|$ at $\varphi = 0°$ (e) $|E_\theta|$ at $\varphi = 0°$.

C. Verification of the SSM by Measuring the Difference Pattern

It is well-known that monopulse antennas are widely used in radar systems for tracking purposes. Depending on the design goal, a deference pattern can be made in both azimuth and elevation planes. Detecting the null position in deference pattern and slope value of the beam around the null position, which all have a direct effect on the angle tracking error, are the main challenges in the pattern measurement of these antennas. For example, if the aperture size of a radar antenna is large in the azimuth plane (similar to that presented in Fig. 7) and the antenna is designed to radiate an azimuth difference pattern, the resulted monopulse pattern will be formed in the azimuth plane with a narrow beamwidth. In this fashion, antenna pattern measurement in the azimuth plane is difficult with the CNF system. This is why a large number of CMCs is required to accurately describe the far-field pattern. Therefore, as mentioned before, the measurement

results experience considerable errors if the conventional cylindrical scanning method is used.

In this subsection, an azimuth difference pattern with narrow beamwidth is generated by properly exciting the array elements described in section B. Afterward, the far-field radiation pattern is calculated with and without using the SSM in the CNF system to further highlight the advantage of the SSM to calculate the difference pattern with high accuracy, especially around the null position. In doing so, Taylor and Bayliss distributions in the elevation and azimuth planes are considered respectively as the desired excitation functions. For both Taylor and Bayliss functions, $\bar{n}$ and sidelobe levels are considered 4 and -40 dB, respectively. Fig. 11 shows the normalized excitation current distribution of the array to generate a difference pattern in the azimuth plane. Near-field components including E_z and E_ϕ are sampled on a cylinder with the radius and height equal to 1.15m and 2m, respectively as shown in Fig. 12. It can be observed that E_ϕ component has a null in the front side of the antenna which leads to the generation of a null in the far zone. Also, E_ϕ is a stronger field than E_z on the cylinder indicating that the major contribution of the far-field pattern is provided by E_ϕ.
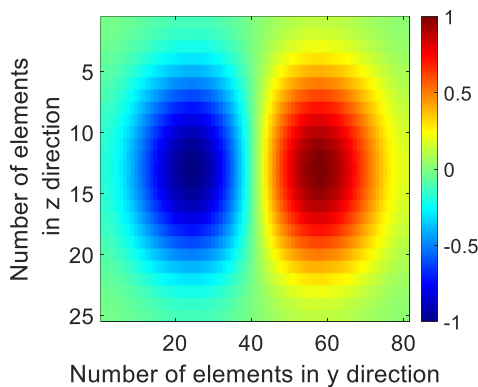
Fig. 11: Excitation current distribution of the array with the configuration shown in Fig. 7.
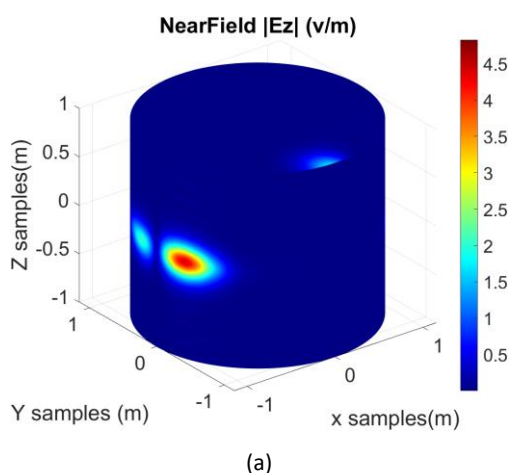
(a)
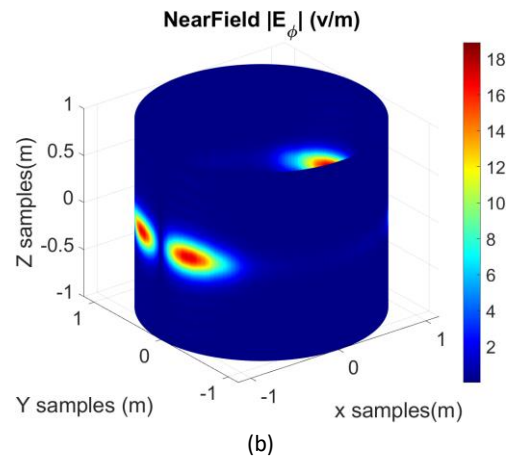
(b)

Fig. 12: Near-field components of the electric field on the scanning cylinder.

As the sampling step varies from 0.9° to 0.1°, the observations are similar to those presented for the sum pattern in Fig. 9. To conserve space, the far-field results have not been presented in this subsection. A proper explanation that can be given in this regard is that when $\Delta\varphi$ is considered as 0.9°, it can be inferred that the near-field-to-far-field transformation cannot predict the radiation pattern accurately. When the sampling step is reduced from 0.9° to 0.5°, the resulted pattern will be more accurate; but as the sampling step decrease from 0.5° to 0.1°, a considerable error is observed in the results. The reason behind this fact comes from the inaccuracy of calculating the CMCs during the transformation of the near-field data to the far-field pattern as the number of modes increases. Furthermore, the error due to the use of more CMCs in the far-field calculation process is much greater than the error due to the use of large step sizes in data acquisition.

Note that this error affects the angle tracking error because the slope and position of the null in the difference pattern suffer some errors. Our investigations show that this error enhances when the beam is scanned. To prove this claim, a scanned beam is generated by the array and the far-field pattern of the antenna is calculated by two techniques, i.e., array theory and the classical CNF method. To do this, a given progressive phase is applied to the rows and columns of the array to scan the beam in the elevation and azimuth planes by 20° and 15°, respectively. It is found that the pattern in the side-lobe region along with the null position of the main beam and slope of the beam around the null include some errors which are more than the errors in broadside radiation.

In light of the above discussion, the need for an accurate method to calculate the difference pattern for all beam directions is inevitable. The classical CNF suffers from inaccuracy and the SSM technique can significantly enhance the measurement accuracy. Fig. 13 shows the far-field pattern of the antenna by the use of the SSM. In

112

J. Electr. Comput. Eng. Innovations, 11(1): 103-118, 2023

the SSM, $\Delta\varphi_{Data\ acquisition} = 0.1°$ and $\Delta\varphi_{seq} = 0.5$, $N_{seq} = 5$ are considered. In this design, the null position is considered at the broadside. It is observed that both co-pol and cross-pol patterns are calculated properly when compared with the ideal results.

(a)

(b)

(c)

(d)

(e)
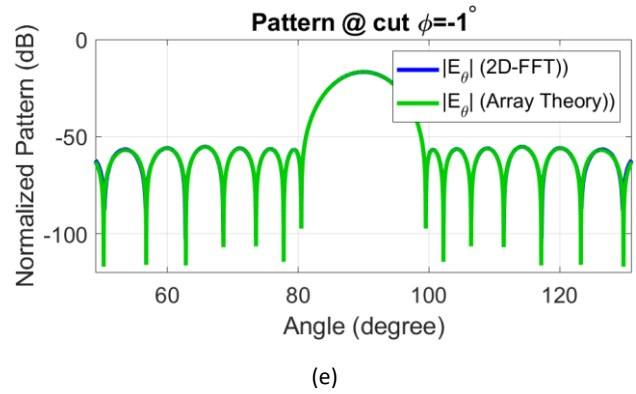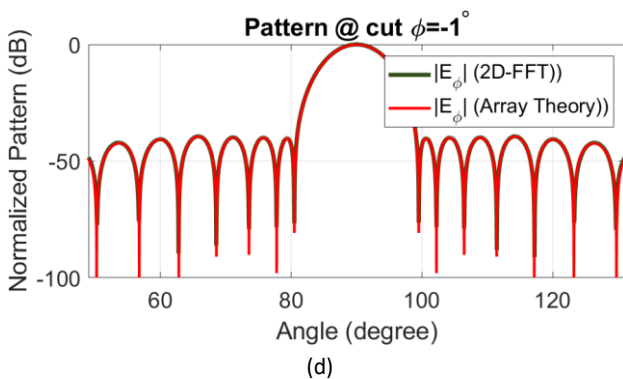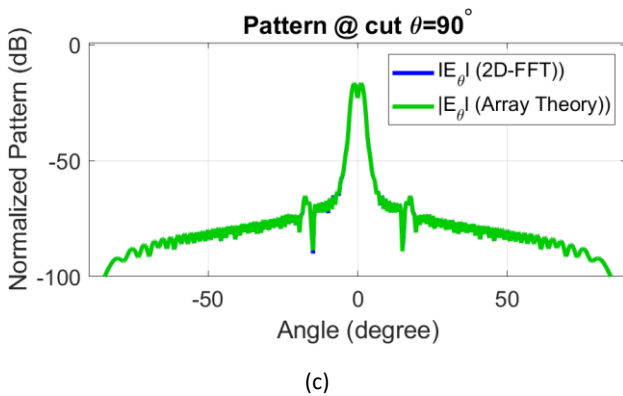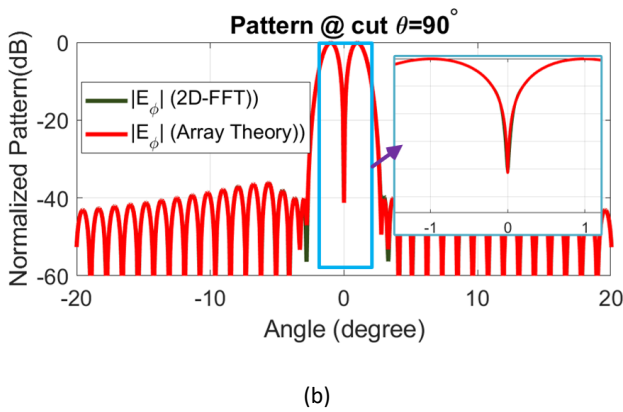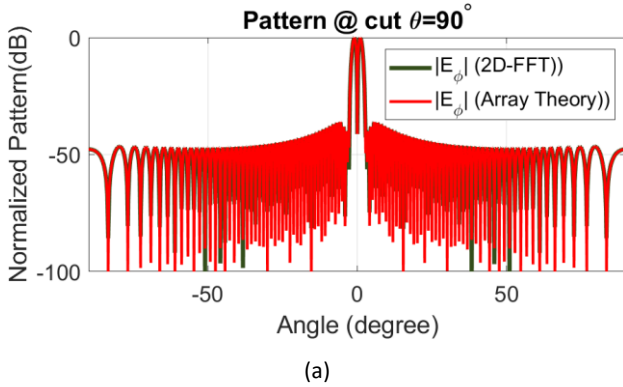
Fig. 13: The comparison between the far-field results of the difference pattern obtained by ideal array theory and the CNF system by using the SSM. $\Delta\varphi_{Data\ acquisition} = 0.1°$ and $\Delta\varphi_{seq} = 0.5$, $N_{seq} = 5$. (a) $|E_\varphi|$ at $\theta = 90°$. (b) closer view of $|E_\varphi|$ at $\theta = 90°$. (c) $|E_\theta|$ at $\theta = 90°$ (d) $|E_\varphi|$ at $\varphi = -1°$ (e) $|E_\theta|$ at $\varphi = -1°$.

Reducing Data Acquisition and Single-Cut Measurement Criteria in CNF system with the SSM

Reducing the data acquisition process is of interest in many mass production scenarios in which many identical antennas need to be measured. This work is performed by eliminating unnecessary data in the near-field region. For example, if the position and slope of the null in a monopulse pattern are required, there is no need to completely sample all of the near-field data in the three-dimensional space.

Equivalently, the shape of the main beam and first sidelobe levels are related to the near-field data on the front side of the antenna. This issue is also valid for necessary components of the electric field (E_z or E_φ or both of them) which should be sampled based on the required information about the pattern. (I) Reducing the sampling area to a sector with a given central angle, (II) single-cut measurement, (III) and choosing the necessary components of the electric field as desired, all significantly accelerate the pattern measurement process. Furthermore, in the factory calibration process of electrically large scanned-beam active phased array antennas, the fast and single-cut measurement would be helpful to find the possible errors in the antenna configuration very quickly. The CNF system in conjunction with the SSM is a good candidate to accomplish this task with acceptable accuracy. The CNF system in its simplest form can be employed as a single-cut measurement technique which is named the zero-height CNF system. The near-field-to-far-field transformation is done over a zero-height ring enclosing the AUT. In this section, several scenarios including sector sampling and single-cut sampling are investigated by the CNF system in conjunction with the SSM to determine the required criteria for reducing the unnecessary near-field data.

A. CNF and SSM based on Sector Sampling Area

The combination of the CNF and SSM as a powerful solution to characterize the antenna radiation pattern can be employed to determine the amount of near-field data required to fully describe the radiation field in the front of the antenna with minimal error. Fig. 14 shows the sector sampling scenario for pattern measurement of antenna described in the previous section. The results are presented in Fig. 15 up to Fig. 17 for various values of α angle (α=50° and α=120°).
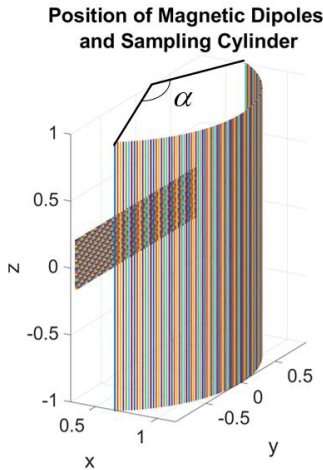
Fig. 14: Sector sampling area subtended by α angle.

It can be observed from Fig. 15 up to Fig. 17 that as far as the far-field on the front side of the antenna is concerned, one can extract the near-field data on a sector area with the subtended angle of α=120° around the peak value of the beam in the azimuth pattern. This fact is also valid for other types of antennas with narrow beamwidth in the azimuth plane and it is possible to find the minimum value of α angle to characterize the beam in front side of the antenna by the CNF system and SSM. Note that, if the SSM is not used to calculate the fields, the results will not be valid at all and we cannot determine the desired subtended angle, α, associated with the sampling sector area to accurately calculate the far-field patterns.

(b)
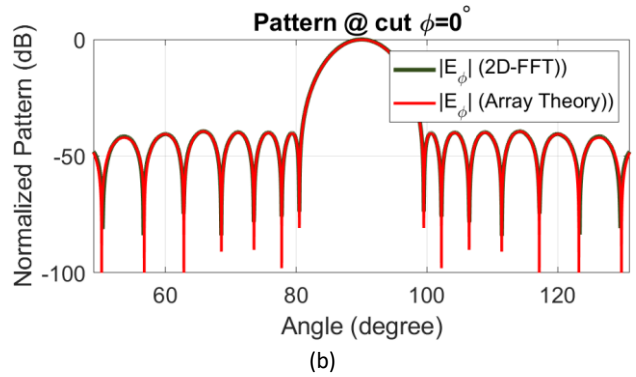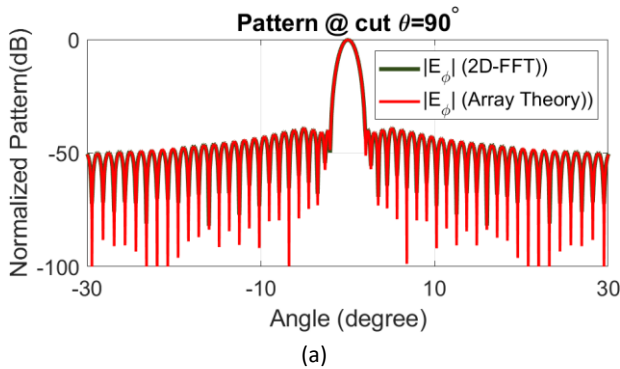
Fig. 15: Co-pol components of the pattern obtained by the sector sampling scenario with α=120° in (a) azimuth (b) elevation planes.

(a)

(b)
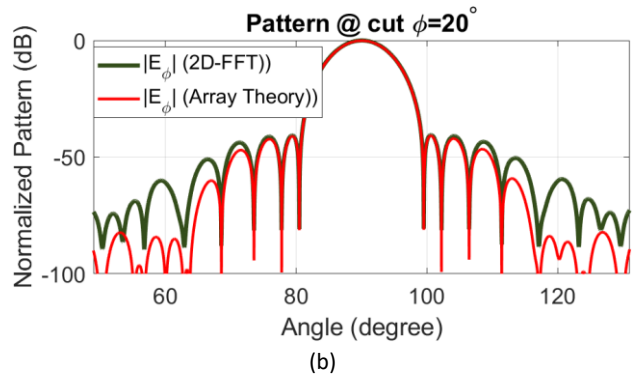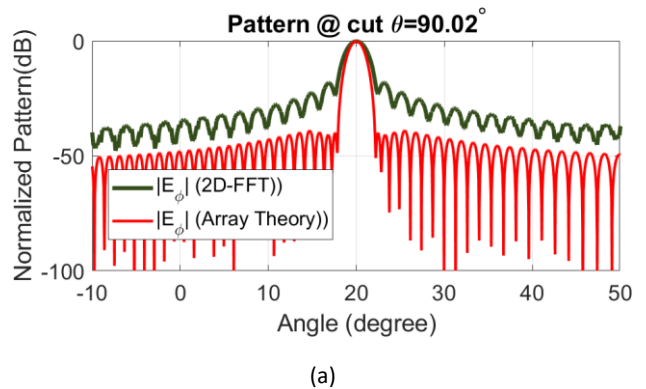
Fig. 16: Co-pol component results of a scanned beam pattern obtained by sector sampling scenario with α=50° in (a) azimuth (b) elevation planes. The beam is scanned to $\varphi = 20°$.

(a)

(a)

(b)
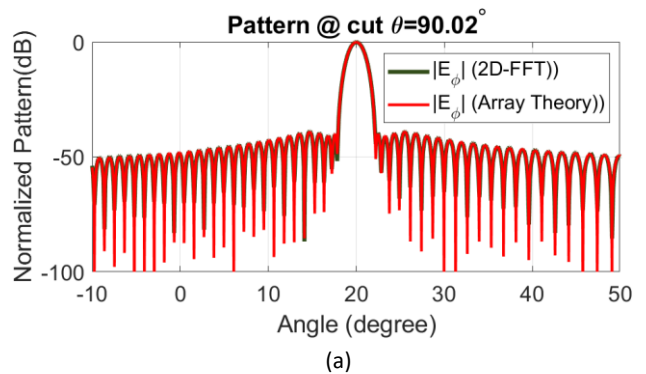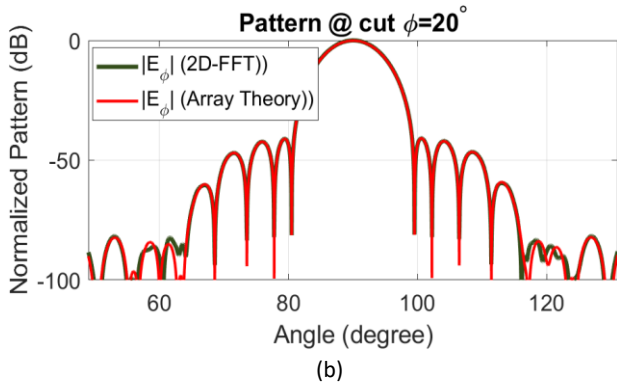
Fig. 17: Co-pol components of a scanned beam obtained by sector sampling scenario with α=120° in (a) azimuth (b) elevation planes. The beam is scanned to $\varphi = 20°$.

The results show that if we sampled a sector area around the main beam with the subtended angle equal to 120°, the calculated radiation pattern in the front side of the AUT has a good agreement with the ideal pattern. This argument can be made for other AUT with different beamwidth and beam directions and optimal subtended angle related to the sampling sector would be obtained based on the desired accuracy.

B. CNF and SSM based on Single-Cut Data Acquisition

As a special case of three-dimensional cylindrical scanning measurement, single-cut measurement (SCM) along the z and φ directions are an interesting solution to characterize the antenna patterns [20]. In general, the SCM drastically reduces the testing time; however, this technique is not useful for any type of antenna. For example, the authors in [23] exploited the SCM technique to characterize a large size one-dimensional array antenna (based station antenna as a practical case), in which the pattern is wide in the azimuth plane and directional in the elevation plane. In this fashion, the testing time can further be decreased by using multi-probe measurement, because the measurement is done only in one dimension [24]-[30].

Generally, the SCM can be implemented by the CNF system in two different states: (I) linear moving of the probe along the z-direction and (II) moving the probe in the φ- direction. The latter state is well-known as a zero-height CNF measurement. In classical CNF, it is difficult to apply the SCM scenario in the φ- direction due to the limitation of the CNF system in the measurement of the patterns with narrow beamwidth in the azimuth plane, hence, in this state the antenna should necessarily be rotated by 90° to accomplish the sampling process over a single zero-height ring enclosing the antenna. In the vast majority of cases, it is impossible to rotate the antenna because of mechanical limitations. The SSM can be effectively used to overcome this drawback. To implement the SCM, it is enough to apply a one-

dimensional fast Fourier transform (1D-FFT) in the Near-field-to-far-field transformation process. Fig. 18 shows two possible SCM scenarios developed by the CNF system and the SSM. By sampling the near-field data along the z-axis, the pattern will be calculated in the elevation plane. Similarly, sampling over the ring enclosing the antenna leads to calculating the pattern in the azimuth plane.

(a)
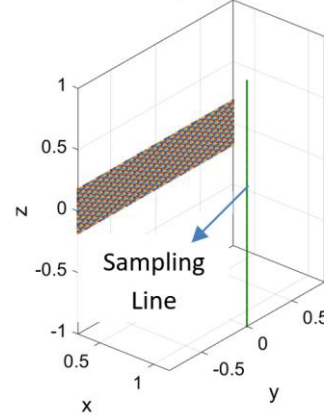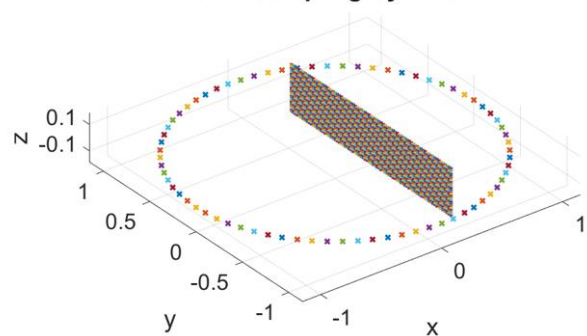
(b)

Fig. 18: Two scenarios of the SCM developed by CNF and the SSM.

(a)

(b)
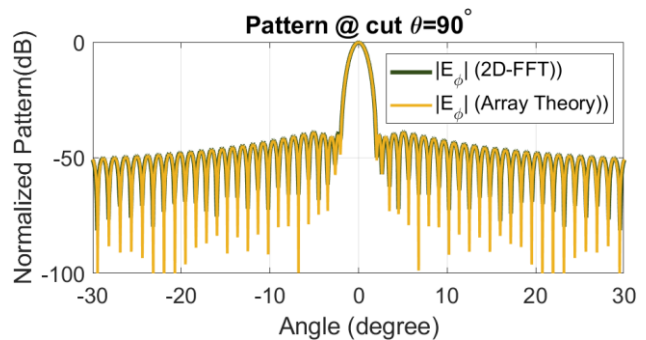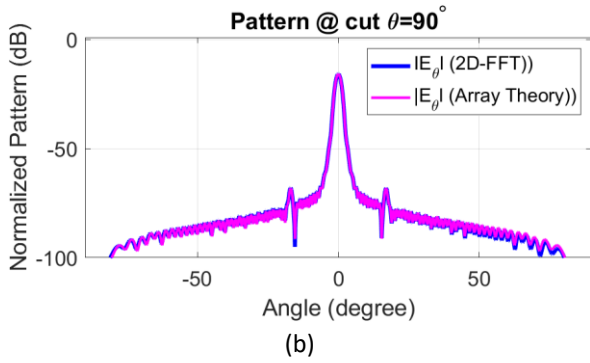
Fig. 19: The far-field pattern resulted from the SCM by scanning the near-field data over the straight line shown in Fig. 18(a).

(a)

(b)
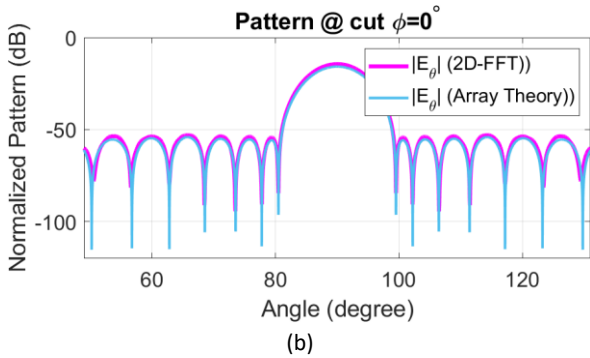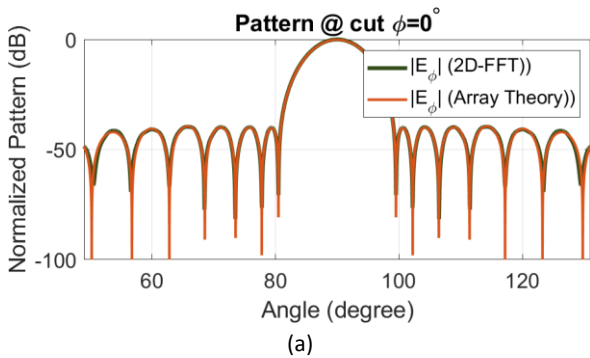
Fig. 20: Far-field pattern resulted from the SSM by scanning the near-field data over the ring shown in Fig. 18 (b).

The far-field results are presented in Fig. 19 and Fig. 20. It can be observed that if the near-field data are recorded over the zero-height ring, the azimuth pattern can effectively be estimated by the CNF and SSM. In addition, if the near-field data are recorded along the z-axis, the elevation pattern will be estimated with acceptable accuracy.

Comparison and Discussion

To complete the discussion, a comparison is accomplished between the CNF measurement system developed in this work and the previously reported works which is presented in Table 1. As can be seen, the authors in [13] tested a very large L-band radar antenna by a CNF system. The AUT in [13] has a sum pattern (with half-power beamwidth less than 2°) in the horizontal cut and a difference pattern in the elevation cut. To measure the sum pattern in the azimuth plane and characterize the

main beam direction with the acceptable error, 512 samples are selected in the φ-direction. Apparently, if the deference pattern was in the azimuth plane, much more points would have to be taken. in the azimuth plane in [13]. Two other works listed in Table 1, that is [21] and [22], are related to the measurement of antennas with a wide-angle beam in the azimuth plane. As shown in Table 1, the sampling steps in [21] and [22] are selected to be 6° and 2.5°, respectively which are much larger than the sampling step used in [13] because of wider beamwidth.

A closer examination of the achievements presented in [22] verifies the fact that higher-order Henkel functions are required for data acquisition if the azimuth beamwidth is small. This ultimately leads to smaller sampling steps. The authors in [22] measured a horn antenna wide wide-angle beam as the first practical case with CNF system by applying the Hankel function with the order up to 44 leading to $\Delta\phi = 4°$. In the second case, a dish antenna was utilized as the AUT and the azimuth pattern was measured by applying the Hankel function with the order up to 72 leading to $\Delta\phi = 2.5°$ as depicted in Table 1.

Table 1: The comparison between the results proposed in this work and the previously published works. H: height, W: width, D: depth. N.R stands for not reported.

Parameter	[13]	[21]	[22]	This work
AUT	L-Band Radar ANT	2- port ANT	Dish ANT	Slot array
Antenna dimension (mm)	large (N.R)	H:2254 W: 259 D: 99	Diameter = 0.34 cm	H: 360 W: 1720
Total Scan Length	7.5 m	2.7 m	990 mm	2 m
Distance probe to AUT	5m~7m	90 cm	20 cm, 40 cm	115 cm
Sampling step	0.7°	6°	2.5°	<0.2°
Sampling Length	10 cm	10 cm	15 mm	10 mm
HPBW in the azimuth	N. R	65°	~10°	1.4°
Sidelobe region estimation capability in the azimuth plane	Very good	weak	Relatively good up to ±20°	excellent
Estimation error of the beam direction in the azimuth plane	≈ 0.1°	Up to 1.19°	N. R	<0.02°

Another comparison is done for SCM which is given in Table 2. It can be seen that a pattern with a half-power beamwidth as small as 1.4° can be measured by the proposed method with excellent compatibility with the theoretical results. This is done by using the small sampling step, 0.2°, thanks to the use of the SSM. Meanwhile, the measurements developed in [20], [23] used the sampling steps equal to 1° to characterize the radiation patterns with broader beamwidths in the azimuth plane. Although, our investigations show that almost SCM systems are used to characterize sum patterns and therefore, proper evaluation and comparison (such as angle tracking error) cannot be done between the presented work and similar ones reported in the literature.

Table 2: The comparison between the results proposed in this work for SCM and the previously published works. H: height, W: width, D: depth. N.R stands for not reported.

Parameter	[20]	[23]	This work
AUT	LPDA	Sector ANT	Slot array
Antenna dimension (mm)	N. R	H: 834 mm	H: 360 W: 1720
Distance probe to AUT	91cm	10 cm	115 cm
Sampling step	1°	1°	<0.2°
HPBW in the azimuth	N. R	>50°	1.4°
Sidelobe region estimation capability in the azimuth plane	weak	Relatively good up to ±60°	excellent
Estimation error of the beam direction in the azimuth plane	N. R	N. R	<0.02°

Conclusion

In this paper, a novel method named the SSM is introduced to circumvent the serious limitation of the CNF measurement system and characterize the antenna pattern with narrow beamwidth in the azimuth plane. The presented method is based on artfully selecting the φ angle sequences and calculating the associated patterns in a repetitive routine. To verify the SSM, a comprehensive analytical model based on coordinate transformation with Euler angles is presented, which is useful to characterize the radiation pattern of every array antenna consisting of slot or microstrip patch elements.

Author Contributions

This paper is fully prepared by Majid Karimipour, assistant professor at the Arak University of Technology. The primitive idea, mathematical calculations, Matlab code, and simulations are all accomplished by Majid Karimipour.

Conflict of Interest

The author declares that there is no conflict of interest regarding the publication of this manuscript. In addition, the ethical issues, including plagiarism, informed consent, misconduct, data fabrication and/or falsification, double publication and/or submission, and redundancy have been completely observed by the authors.

Abbreviations

SSM	Sequential Sampling Method
Co-Pol	Co Polarization
Cross-Pol	Cross Polarization
CNF	Cylindrical Near-Field
FFT	Fast Fourier Transform
CMC	Cylindrical Mode Coefficient
2D	Two Dimensional
3D	Three Dimensional
AUT	Antenna Under Test
SCM	Single-Cut Measurement

Reference

[1] C. Parirni, S. Gregson, G. MacCormick, D. J. Van Rensburg, T. Eibert, Theory and Practice of Modern Antenna Range Measurements, v2, London: IET, 2020.

[2] A. D. Yaghjian, "An overview of near-field antenna measurements", IEEE Trans. Antennas Propag., 34(1): 30-45, 1986.

[3] A. Taaghol, T. K. Sarkar, "Near-field to near/far-field transformation for arbitrary near-field geometry, utilizing an equivalent magnetic current," IEEE Trans. Electromagn. Compat., 38(3): 536–542, 1996.

[4] M. Salucci, M. D. Migliore, P. Rocca, A. Polo, A. Massa, " Reliable antenna measurements in a near-field cylindrical setup with a sparsity promoting approach," IEEE Trans. Antennas Propag., 68(5): 4143-4148, 2020.

[5] J. S. Row, J. F. Tsai, "Cylindrical near-field antenna measurement using a polarization reconfigurable probe," Microwave Opt. Technol. Lett., 58(11): 2707–2711, 2016.

[6] F. R. Varela, M. J. L. Morales, R. T. Sanchez, A. T. M. Barrado, E. d. l. F. González, G. P. Quijano, C. Z. Torres, M. S. Pérez, M. S. Castañer, "Multi-probe measurement multi-probe measurement system based on single-cut transformation for fast testing of linear arrays," Sensors, 1744(21): 1-14, 2021.

[7] C. Apriono, Nofrizal, M. D. Firmansyah, F. Y. Zulkifli, E. T. Rahardjo, "Near-field to far-field transformation of cylindrical scanning antenna measurement using two dimension fast-fourier transform," Int. Conf. Qual. Res., 368-371, 2017.

[8] M. Farouq, M. Serhir, D. Picard, "Matrix method for far-field calculation using irregular near-field samples for cylindrical and spherical scanning surfaces," Prog. Electromagn. Res. Lett B., 63: 35–48, 2015.

[9] C. H, Schmidt, T. F. Eibert, "Assessment of irregular sampling near-field far-field transformation employing plane-wave field representation," IEEE Antennas Propag. Mag., 53(3): 213–219, 2011.

[10] O. M. Bucci, C. Gennarelli, C. Savarese, "Interpolation of electromagnetic radiated fields over a plane by nonuniform samples," IEEE Trans. Antennas Propag., 41(11): 1501–1508, 1993.

[11] A. Capozzoli, C. Curcio, A. Liseno, "Optimized near field antenna measurements in the cylindrical geometry," presented at the European Conf on Antennas. Propag, EUCAP., Lisbon, Portugal, 2015.

[12] https://www.nsi-mi.com/products/system-solutions/near-field-systems.

[13] S. Burgos, F. Martin, J. L. Besada," Cylindrical near-to-far-field transformation system for radar antennas: design, validation, and application," Microw. Opt. Technol. Lett., 50(10): 2527–2531, 2008.

[14] L. Jossefson, S. R. Rengarajan, Slotted Waveguide Array Antennas: Theory, analysis and design, vol. 1, London: Wiley, 2018.

[15] C. Balanis, Antenna theory: analysis and design, Hoboken, N.J.: Wiley-Interscience, 2016.

[16] Y. Rahmat-Samii, "Useful coordinate transformations for antenna applications." IEEE Trans. Antennas and Propag., (27)4, 571-574, 1979.

[17] B. Fuchs, L. L, Coq, M. D. Migliore, "On the interpolation of electromagnetic near field without prior knowledge of the radiating source," IEEE Trans. Antennas Propag., 65(7): 3568–3574, 2017.

[18] M. D. Migliore, "Near field antenna measurement sampling strategies: From linear to nonlinear interpolation," Electronics, 7(10): 1-21, 2018.

[19] Y. Hayashi, H. Arai "A reduction of measurement points in cylindrical near field measurement by complex interpolation," Int. Symp. on Antennas and Propag., Osaka, Japan, 2021.

[20] S. Omi, T. Uno, T. Arima, "Single-Cut near-field far-field transformation technique employing two-dimensional plane-wave expansion," IEEE Antennas Wirel. Propag. Lett., 17(8): 1538-1541, 2018.

[21] K. Phaebua, T. Lertwiriyaprapa, D. Torrungrueng, "Cylindrical near-field to far-field radiation pattern measurement system for a large mobile phone base station antenna," presented at the 2021 Int. Electr. Eng. Congr.,:10-12, Pattaya, THAILAND, 2021.

[22] J. Puskely, "Application of iterative fourier method in cylindrical phaseless antenna measurement technique," Radioengineering, 21(1): 422-429, 2012.

[23] Y. Sugimoto, H. Arai, T. Maruyama, M. Nasuno, M. Hirose, S. Kurokawa, "Fast far-field estimation method by compact single cut near-field measurements for electrically long antenna array," IEEE Trans. Antennas Propag., 66(11): 5859-5868, 2018.

[24] M. Sierra-Castañer, "Review of recent advances and future challenges in antenna measurement," Appl. Comput. Electromagn. Soc. J., 33(1): 99-102, 2018.

[25] R. Cornelius, T. Salmerón-Ruiz, F. Saccardi, L. Foged, D. Heberling, M. Sierra-Castañer, "A comparison of different methods for fast single-cut near-to-far-field transformation," IEEE Antennas Propag Mag., 56(2): 252-261, 2014.

[26] X. Li, G. Wei, L. Yang, B. Liao, "Fast determination of single-cut far-field pattern of base station antenna at a quasi-far-field distance," IEEE Trans. Antennas and Propag., 68(5): 3989-3996, 2020.

[27] F. R. Varela, R. T. Sánchez, M.J.L. Morales, M. Sierra-Castañer, "Near-field to far-field transformation for fast linear slide measurements" presented at the 14th Eur. Conf. antennas Propag. EuCAP Copenhagen, Denmark, 2020.

[28] L. J. Foged, G. Barone, F. Saccardi, "Antenna measurement systems using multi-probe technology," presented at the IEEE Conf. Antenna Meas. Appl. Chiang Mai, Thailand, 2015.

[29] F. Las-Heras, B. Galocha, J. L. Besada, "Far-field performance of linear antennas determined from near-field data," IEEE Trans. Antennas Propag., 50(3): 408-410, 2002.

[30] M. Orefice, M. A. Razzaq, G. Dassano, "Sidelobe level correction for parabolic antennas radiation pattern measurements in quasi-far-field conditions", Electron. Lett., 49(23): 1423-1425, 2013.

Biographies

Majid Karimipour received his B. Sc., M.Sc., and Ph.D. degrees all in Electrical Engineering in 2010, 2013, and 2018, respectively. The title of his Ph.D. thesis was " The application of the holographic technique in the synthesis of antenna radiation pattern" which was defened in the Iran University of Technology (IUST) with excellent grades. From 2014 to 2018 he worked with the communication satellite group, Iran Telecommunication Research Center, (ITRC) in Tehran, Iran, as a major researcher. He is currently an assistant professor with the Arak University of Technology. He has high experience in antenna near-field measurement and calibration systems, especially planar and cylindrical scanning systems. He has taught, communication systems, antenna theory, signal and system, and electromagnetic courses since 2015. His major research interests are the development and design of reflect array and transmit array antennas, phased array antennas, pattern synthesis, and near-field antenna pattern measurement systems.

- Email: m.karimipour@arakut.ac.ir
- ORCID: 0000-0001-7612-2512
- Web of Science Researcher ID: CAG-4398-2022
- Scopus Author ID: 55962138900
- Homepage: https://scholar.google.com/citations?user=3rZQKjAAAAAJ&hl=en